Study on the seismic performance of retrofitted RC frames with RC infill wall mega braces

Shao-Ge Cheng [a], Yi-Xiu Zhu [b,*], Wei-Ping Zhang [b], Tie-Hua Shi [a]

[a] *China Academy of Building Research, Institute of Earthquake Engineering, 30 East North Third Ring Road, Beijing 100013, China*
[b] *College of Civil Engineering, Tongji University, 1239 Siping Road, Shanghai 200092, China*

ABSTRACT

This paper proposes a novel arrangement of RC infill walls made possible by RC infill wall mega braces (RCIWMBs). The seismic behavior of a reinforced concrete (RC) frame structure retrofitted by the RCIWMB was investigated through 1/5-scale shaking table tests. The seismic damage characteristics and the dynamic responses of the model structure under different input ground motions are presented in detail. The results show that the presence of the RCIWMB has a slight effect on the failure of beam-column joints, but it can lead to punching shear failure of its connected frame columns. When the RC walls are arranged diagonally, the RCIWMB can form a macroscopic brace effect, serving as the first seismic line of defense. Compared with traditional RC infill wall retrofitted frame structures, the drawback is obvious failure, which appears on the lower stories of this novel type of structure and is prone to forming a weak story. This indicates a poor structural story ductility and more severe damage to the integral structure. However, the addition of the RCIWMB resulted in a substantial increase in the integral lateral bearing capacity, integral lateral stiffness and integral ductile behavior, a decrease in lateral displacement, and a reduction in damage to the original frame structure. The novel structural system performed better under extensive seismic tests, providing a new method for upgrading the seismic performance of existing buildings.

1. Introduction

Reinforced concrete (RC) frame structures have been widely used worldwide in multistory buildings because of their light weight, flexible space division and material savings. In recent years, earthquakes have inflicted severe damage, including collapse, on many RC frame structures because of their lack of sufficient ductility, bearing capacity, and energy dissipation capacity [1,2]. Although there are many novel strengthening methods for RC framed structures [3–7], such as using cross laminated timber panels as infill shear walls, the addition of RC infill walls remains a relatively feasible and popular technique for retrofitting existing RC buildings, which do not comply with current seismic requirements [8–10]. Tests and numerical simulation studies on the seismic performance of RC frame structures infilled with RC walls have been conducted by many researchers who typically handle the RC wall frame design by aligning RC infill walls in a continuous arrangement in a multistory building from the bottom to the top [11–14]. Previous studies have shown that adding RC walls can effectively improve the lateral stiffness and bearing capacity of a structure, thereby

limiting its displacement. However, structural engineers have found it more advantageous to stagger the RC walls as they evenly disperse them along the building's height, similar to the inclined web members of a truss, rather than continuously extending the shear walls from the bottom to the top [15–19]. Few shaking table tests have been conducted to test RC frames retrofitted with staggered RC infill walls; thus, the understanding of the seismic behavior of this arrangement is limited. Therefore, a shaking table test was used to measure the seismic performance of the retrofitted RC frames under earthquake conditions and provide more reliable information on their structural mechanics and behaviors.

To shed light on the seismic performance of an RC frame structure with staggered RC infill walls, a 1/5-scale shaking table test was conducted at the State Key Laboratory of Building Safety and Environment in the China Academy of Building Research in Beijing. The RC frame used for testing represents a low-strength concrete frame structure built in China in the 1970s. The RC infill walls were staggered diagonally without a break from the bottom story to the top story in the axes of the RC frame's structural facade, forming a macro RC infill wall (with) mega

braces (RCIWMBs). No foundation was set for the RC infill walls. RC infill walls were connected to the frame members through dowel bars all around their perimeter. This novel arrangement of RC infill walls is referred to as the RCIWMB strengthening technique. There are two research objectives in this article: 1) to obtain the seismic performance of an RC frame structure retrofitted with an RCIWMB according to the shaking table test, including failure modes and dynamic responses, and 2) to evaluate the effectiveness of RC frames retrofitted with an RCIWMB by comparing them with a traditional RC infill wall retrofitted frame structure. This paper presents a detailed description of the testing program, test specimen fabrication process, test results, and main observations. The authors also include recommendations pertaining to the potential use of the novel retrofitting techniques introduced herein.

2. Studied building

The studied frame building is located in an 8-degree-seismic design area, Group 1, at a Class III site, according to Chinese standard GB50011-2010 [20]. In addition to the self-weight of the RC frame structure, the permanent load weight was 5480 kN on the first story, 5290 kN on the second to fourth stories, and 4270 kN on the fifth story.

The total height of the frame structure was 18.4 m, and its plane dimension was 25.2 m × 15 m, as shown in Fig. 1. Three spans were in the transverse direction with center-to-center span lengths of 6 m, 3 m, and 6 m. Seven bays were in the longitudinal direction with a constant center-to-center span length of 3.6 m. The first story of the RC structure had a height of 4.0 m, while the other stories had a constant height of 3.6 m. The frame structure was made to bear an axial compressive strength of C20, which was the standard value equivalent to 13.4 MPa [21]. The floor slab thickness was 120 mm; the section size of the frame column was 450 mm × 450 mm on the first and second stories and 400 mm × 400 mm on the third to fifth stories. The section sizes of the frame beams were as follows: The transversal beam (KJL-1) was 300 mm × 600 mm, and the longitudinal beam (KJL-2) was 300 mm × 450 mm. The reinforcement of these frame structural members represents the construction practice of 1970 s China, as specified in Chinese code TJ 11-74 [22].

3. Testing program

3.1. Basic similarity law

The test specimen was designed by scaling down the geometry from the prototype structure. The dimension scaling parameter was taken as 1:5. The main similitude scale factors are listed in Table 1.

3.2. Test model

Fig. 2 shows the model used for the shaking table test performed by our research group on a traditional RC infill wall retrofitted frame structure. A traditional RC infill wall retrofitted frame structure model is referred to as the RC-infill model in this paper. The RC frame structure retrofitted with the RCIWMB tested herein and the RC-infill model have identical geometries. The test model of the novel structural system is shown in Fig. 3. The novel structural model is referred to as the RCB-infill model in this paper.

The RCB-infill model was designed and manufactured based on the abovementioned model dynamic similitude law. The total height of the RCB-infill model is 3.68 m, including a 0.2 m foundation. Its plane dimension is 5.04 m × 3 m.

The additional mass was artificially added to the model on each story, including the 7250 kg additional mass on the first story, the 7020 kg additional mass on the second story, the 7060 kg additional mass on the third and fourth stories, and the 5645 kg additional mass on the fifth story. The C20 strength grade represents the RC frame structural members. The C30 strength grade represents the tested RC infill walls.

Fig. 4 shows the concrete aggregates, brick, and construction process of the RCB-infill model. All the RC frame beams, columns, and slabs were cast in place. The masonry infill walls and the RC infill walls were built after the concrete strength of the frame structure reached 100%.

The 24-mm thick slabs were reinforced using two-layer 2.3 mm steel wire gauze spaced at 25-mm centers in both directions. The design of the frame model reinforcement was based on the similitude of the equivalent yield strength coefficient between an existing building and the model [23]. Reinforcement plans for the model beams and columns are provided in Fig. 5d and e. The 40-mm thick RC infills were reinforced using two-layer 2.6 mm bars spaced at 40 mm centers in both directions. The connection between the RC infills and the frame members was
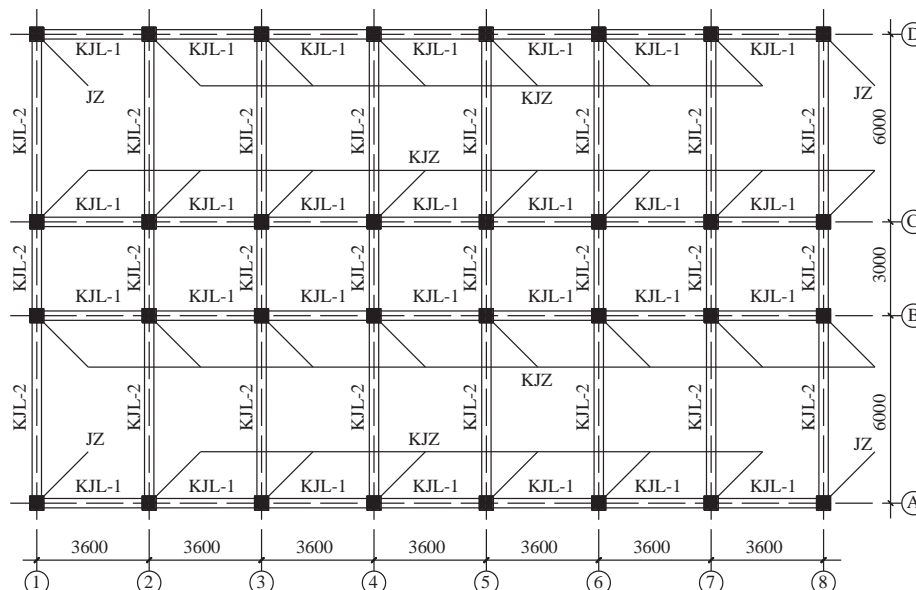

Fig. 1. Plan view of the frame structure.

Table 1
The main similitude scale factor.

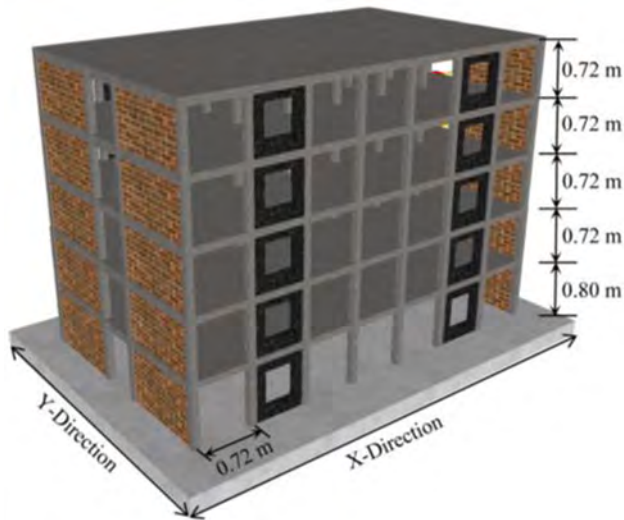| Physical quantity	Similitude law	Model/prototype	Physical quantity	Similitude law	Model/prototype
Length	S_L	1/5	Time	$\sqrt{S_L/S_a}$	1/3.4
Elastic modulus	S_E	1	Horizontal force	$S_E S_L^2$	1/25
Acceleration	S_a	2.3	Frequency	$1/\sqrt{S_L/S_a}$	3.4
Mass	$S_E S_L^2/S_a$	1/57.5	Overturning moment	$S_E S_L^3$	1/125

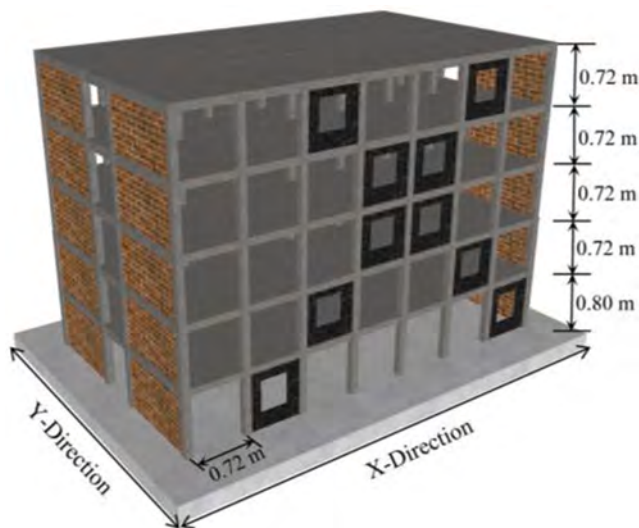**Fig. 2.** RC-infill model.

Fig. 3. RCB-infill model.

achieved by placing dowel bars all around their perimeter, as shown in Fig. 5e.

The construction materials used for the fabrication of the model were selected considering the similarities between the material properties of the model and those of the building used as an example in this study. The microconcrete was used to resemble the concrete of the prototype, and the reinforcement was made of galvanized iron wire. This technique has been widely used in shaking table tests of scaled models [23–25]. Its effectiveness was simulated in the prototype structure performance and proven successful. For the 1/5-scale model, because of the small size of the structural components, the normal concrete could not be poured.

The use of microconcrete with mechanical properties similar to those of traditional concrete materials can effectively solve this problem [26,27]. The concrete mix proportion was identical to that used in this study's existing building example as follows: Portland cement (350 kg/m^3), crushed gravel (1160 kg/m^3), river sand (690 kg/m^3) and fresh water (185 kg/m^3). The scaling parameter of the aggregate diameter was taken as 1:5 (Fig. 4a and b).

Before the test, the mechanical properties of the construction materials used for the fabrication of the test specimen were obtained through the standard test. The measured mechanical properties of the galvanized iron wire are listed in Table 2, and the measured mechanical properties of the microconcrete are listed in Table 3. The concrete was cast layer by layer. Nevertheless, because of the effect of the external environment and construction errors, the concrete properties slightly differ between stories.

3.3. Test procedures

According to Chinese seismic design code GB50011-2010 [20], at least three seismic waves, including at least two real earthquake waves and one artificial wave, must be adopted for dynamic analysis. As shown in Fig. 6 three types of earthquake waves were selected as the input seismic waves, namely, the El Centro wave, Taft wave, and artificial wave.

The El Centro wave and Taft wave were chosen for four reasons: (1) to study the two types of earthquake waves' relatively complete ground motion records, which were collected in the early stages of the earthquake engineering field; (2) to show the two types of earthquake waves because of their wide range of uses for experimental purposes and to compare finite element simulation analyses by many researchers; (3) to raise the comparison ability of these test results with a previous or future similar test; and (4) to achieve the intended research purpose while maintaining versatility, which can complement and perfect this type of shaking table test data and provide a reference for related research. The artificial wave is suited for Group 1 design earthquakes (Class III sites) and is called RD1 for short. To comply with the Chinese seismic design code [15], PGA was applied as the intensity measure for scaling, and the peak ground accelerations (PGAs) were temporarily set at 1 gal (0.01 m/s^2 or 0.001 g). The input PGA level was adjusted according to the seismic intensity requirement [28]. The natural frequencies and the relevant vibrational mode were obtained using white noise before and after each earthquake excitation. Earthquake waves were used to excite the model during various stages of the test, to push the structure from elastic to inelastic and severe damage states and to observe their damage patterns.

Table 4 shows the target peak ground acceleration (PGA) intensities of the earthquake sequence at different levels. The case numbers for all white noise sweep tests are not given. The X-direction is the longitudinal direction of the specimen, and the Y-direction is the transverse direction of the specimen (Fig. 3).

During low-amplitude tests (PGA ≤ 115 gal), the three selected earthquake waves were applied in the X- and Y-directions, and the acceleration response under the Taft wave was more violent (PGA = 115 gal); therefore, the Taft wave was used to excite the model in the following tests. The PGA of Test 24 reached 506 gal, so Test 26 was not conducted. Only X-direction tests were conducted to avoid the unacceptable collapse of the specimen from Test 16 to Test 34. After Test 34,
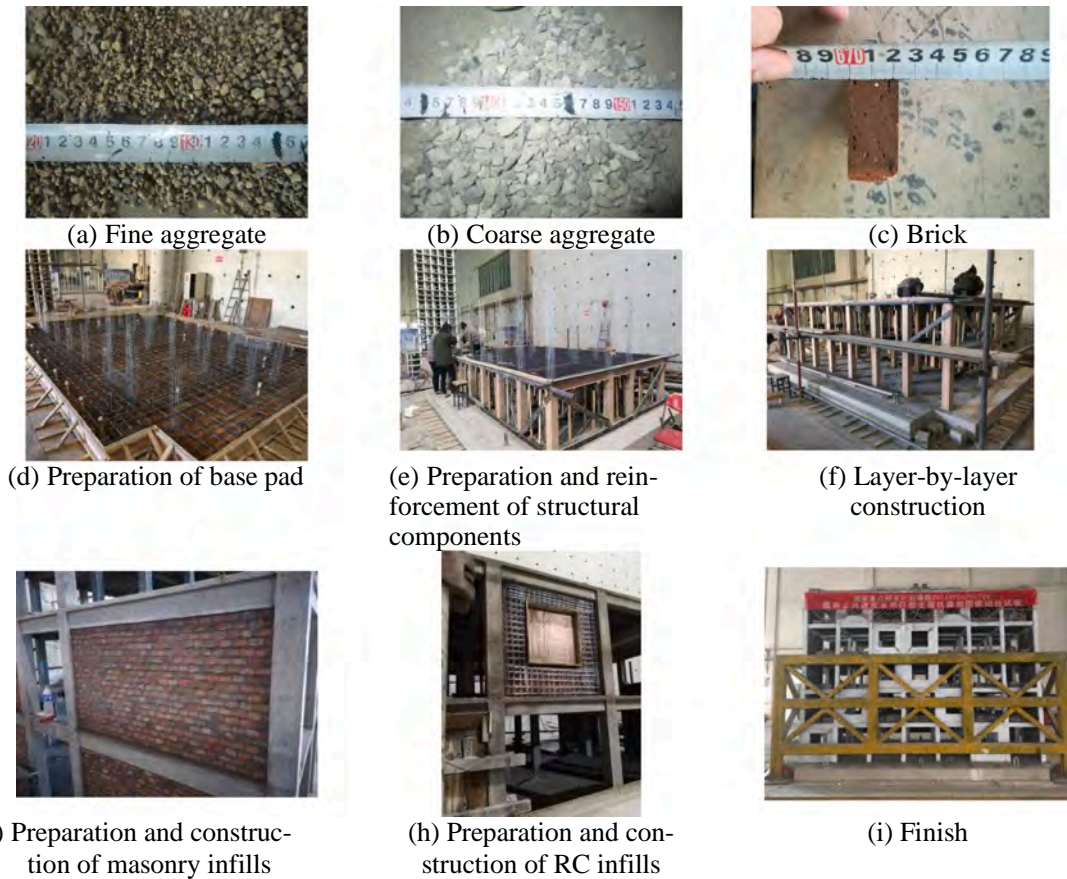
(a) Fine aggregate

(b) Coarse aggregate

(c) Brick

(d) Preparation of base pad

(e) Preparation and reinforcement of structural components

(f) Layer-by-layer construction

(g) Preparation and construction of masonry infills

(h) Preparation and construction of RC infills

(i) Finish

Fig. 4. Construction process of the specimen.

(a) Columns of Stories 1 and 2

(b) Columns of Stories 3 and 4

(c) Columns of Story 5

(d) Beams

(e) Reinforcement details of the RC infill walls
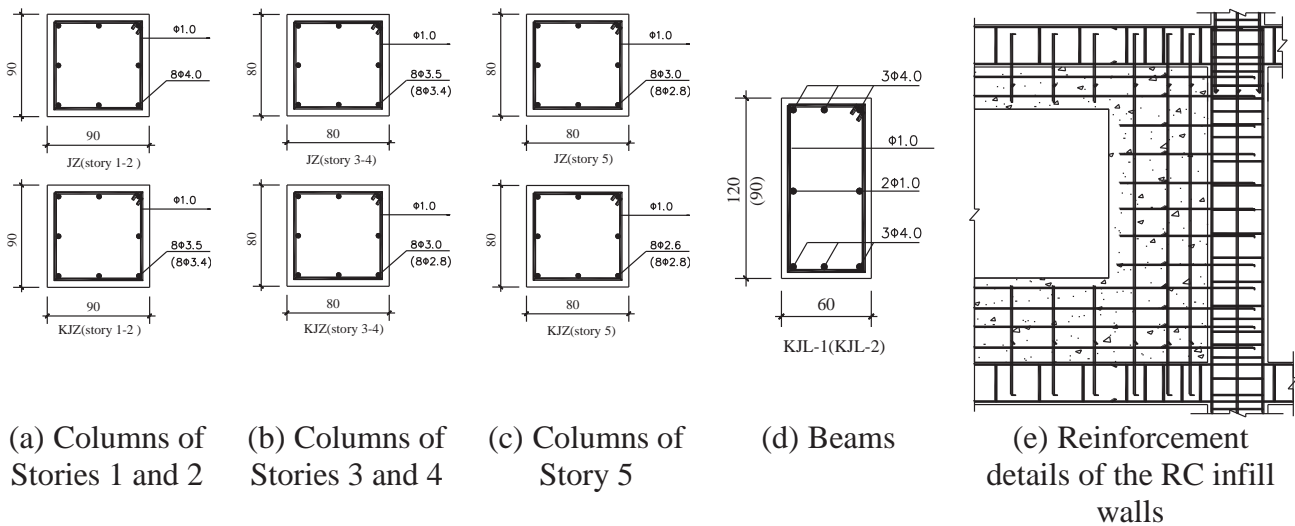
Fig. 5. Reinforcement details for structural members.

Table 2
Mechanical properties of the galvanized iron wire.

Name	d (mm)	Yield strength (MPa)	Young's modulus (MPa)
Galvanized iron wire	4.0	267	181,531
	3.5	302	248,583
	2.6	325	268,299

all longitudinal excitations were completed, and the purpose of this scheduled series of tests was completed. Finally, a few high-amplitude tests were conducted in the Y-direction to observe the types of infill failures; however, few differences were found between the failure mode of the masonry wall and the previous research results [29,30], and the damage no longer propagated in the X-direction for structural components after the three Y-direction tests. Based on these results, the Y-direction tests were not described in detail in this paper.

Table 3

Mechanical properties of the concrete.

Name	Cube compressive strength (MPa)	Young's modulus (MPa)	Description
Microconcrete	26.7	19,900	1st and 2nd stories
	28.3	17,800	3rd and 4th stories
	27.4	19,400	5th story
	25.4	21,600	RC infills
	31.2	25,100	RC infills

3.4. Instrumentation

Accelerometers were placed on the foundation, and each floor slab recorded accelerations in the X- and Y-directions. Twenty-two accelerometers were installed in the test model. The displacement of the model structure was obtained using the acceleration time history integral. Two accelerometers (XS0 and YS0) were arranged on the base in the X- and Y-directions, providing a total of 10 sensors (XS1–XS5, YL1–YL5), which were arranged along the symmetry axis of the X- and Y-directions on the floor slabs. Considering the manufacturing error of the model, the offset of the additional counterweight may have caused the weight asymmetry of the model. Ten accelerometers (XL1–XL5 and YS1–YS5) were also arranged at the end of the X- and Y-directions on the floor slabs. In addition, 34 strainmeters (SL1-SL34) were arranged to measure the dynamic strain response of the frame columns and RC infill walls. The installation locations of these sensors are shown in Fig. 7.

4. Test results

4.1. Damage observations of the RCB-infill model

This work focuses on the seismic performance of the RCB-infill model in the X-direction; therefore, the following damage was primarily associated with the test results of the novel structure in the X-direction.

After the 80-gal excitation, only a few slight cracks were visible in close range, and they developed in the frame beams. After the 115-gal excitation, the initial minor cracks of the RC infills were first observed around the opening. Typical failure modes of the novel structural system in this stage are shown in Fig. 8.

After the 161-gal excitation, we observed newly initiated, slightly inclined cracks and the propagation of cracks on the RC infills. With PGAs ranging from 230 gal to 287.5 gal, an increasing number of new slightly inclined cracks were found in the RC infill walls throughout the 5-story structure. Horizontal cracks appeared at the interface between RC infills and their connected columns in the first story. Fig. 9 shows the typical failure shapes after a PGA reading of 322 gal based on originally formed inclined cracks propagated in the RC infills.

After the 460-gal excitation, the damage degree of the RC walls increased compared with that of the previous working condition, and the inclined cracks began to extend from the edge of the openings to the surrounding frame members. The cracking of the RC walls on the first story was particularly noticeable. The cracks were slight when they
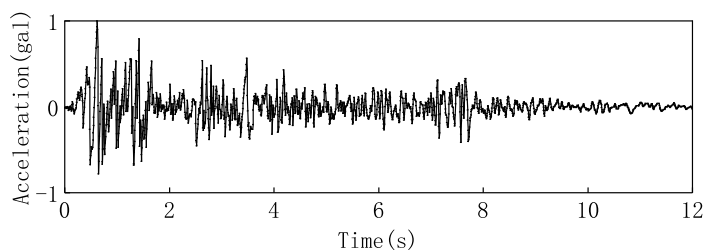
(a) El Centro wave
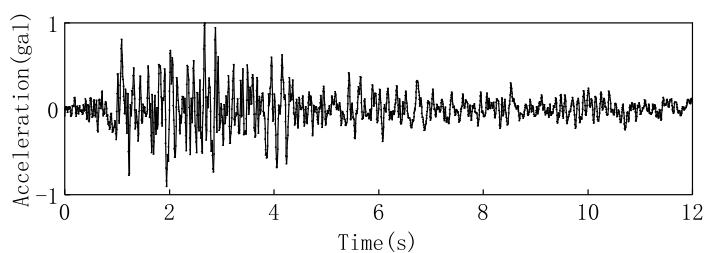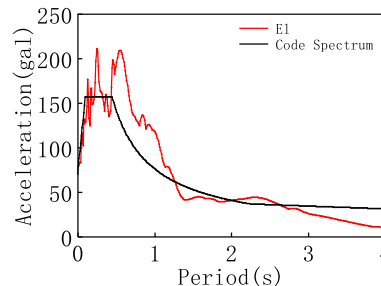
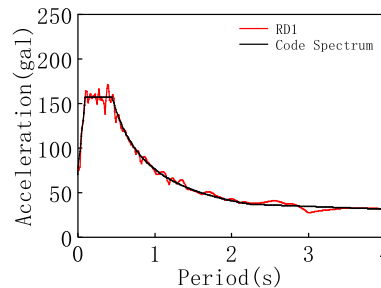(b) Taft wave
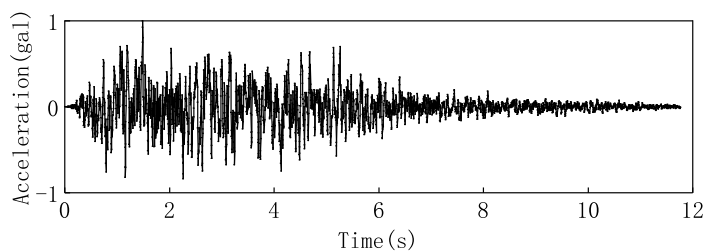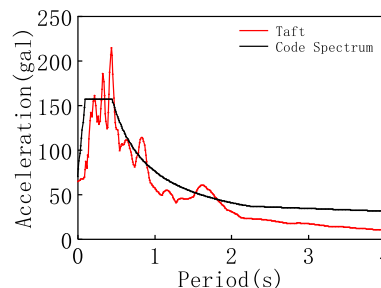
(c) The artificial wave

Fig. 6. Shake-table acceleration response histories and 5%-damped response spectra.

Table 4
Test sequence for the shaking table tests.

Case No.	Ground motion	PGA (gal)	Direction	Case No.	Ground motion	PGA (gal)	Direction
2	RD1	80.5	X	18	Taft	230	X
3	Taft	80.5		20	Taft	287.5	X
4	El Centro	80.5		22	Taft	322	X
5	RD1	80.5	Y	24	Taft	460	X
6	Taft	80.5		26	Taft	506	/
7	El Centro	80.5		28	Taft	690	X
9	RD1	115	X	30	Taft	920	X
10	Taft	115		32	Taft	1173	X
11	El Centro	115		34	Taft	1426	X
12	RD1	115	Y	36	Taft	460	Y
13	Taft	115		38	Taft	690	Y
14	El Centro	115		40	Taft	920	Y
16	Taft	161	X				

(a) A-axis (b) D-axis

Fig. 7. Installation of sensors.
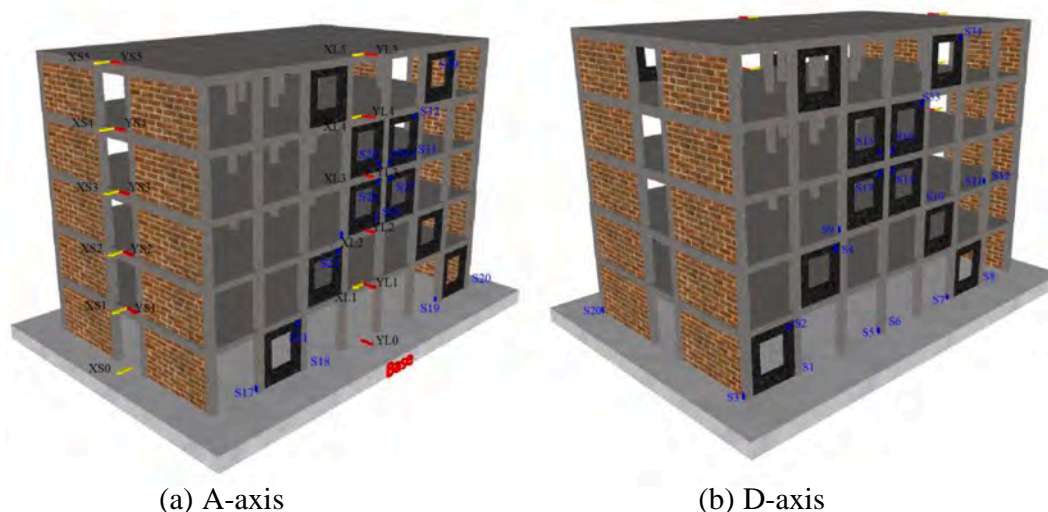

(a) Frame column at the third story (b) RC Infills at the fourth story
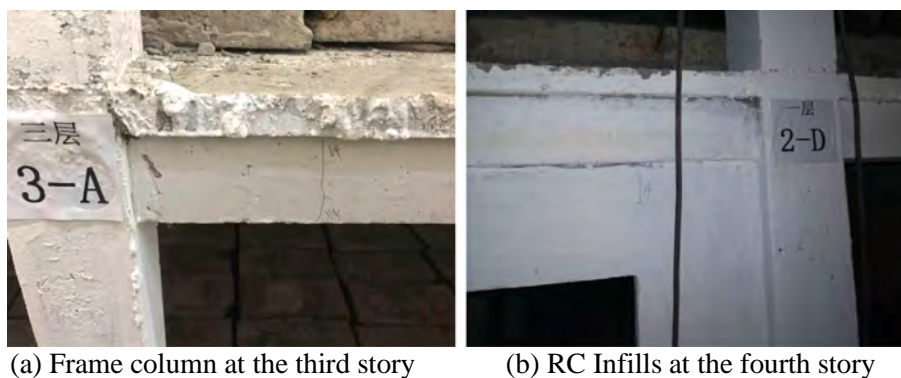
Fig. 8. Typical cracks after the test at PGA = 115 gal.

began to appear in the frame columns. After the RC walls were subjected to PGA = 690 gal, the damage degree of several RC walls increased. Existing cracks expanded and new ones developed. As minor crushing appeared in the RC walls, some of the horizontal penetrating cracks were observed at the column ends, and the number of cracked frame columns increased. After testing at PGA = 920 gal, the concrete was crushed into blocks on the first floor's opening corner of the RC infill wall. The cracks around the opening of the RC walls in other stories were further widened. Obvious horizontal cracks appeared in the upper and lower parts of the connected frame columns. The damage at the top part of the

first-story frame columns became substantial, while the damage to other layers was relatively light. After the test at PGA = 1173 gal, the area of concrete crushing of RC walls in the first story expanded. Concrete cover spalling of RC infills also occurred. Obvious separation appeared at the interface between RC infills and their adjacent columns. Column plastic hinges were formed with spalling of the concrete cover and buckling of the longitudinal reinforcement. After the test at PGA = 1426 gal, the first-story RC infill walls in the RCB-infill model were totally crushed. Punching shear failure and buckling of the reinforcing bars were observed in the adjacent columns. The most severe damage was
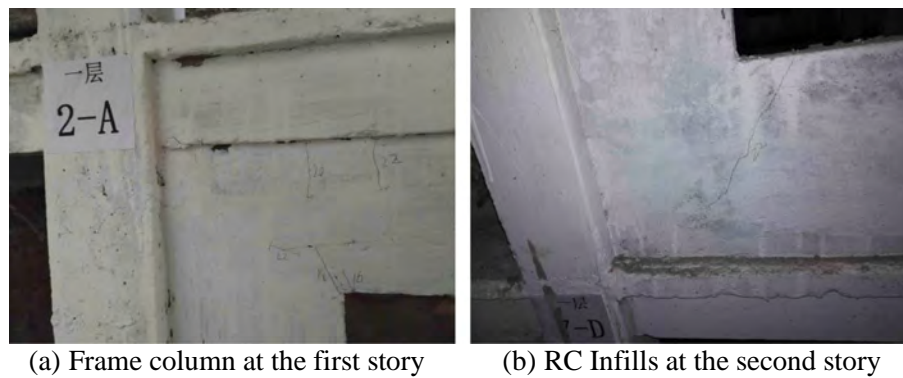
(a) Frame column at the first story (b) RC Infills at the second story

Fig. 9. Typical cracks after the test at PGA = 322 gal.

primarily concentrated in the lower stories, indicating a great possibility of collapse.

4.2. Failure mode comparison

Photographs of the RCB-infill model damage and the RC-infill model after testing are shown in Fig. 10 and Fig. 11, respectively. Substantial shear failure of the frame beam occurred in the RC-infill model but not in the RCB-infill model. Major crack formations clearly showed that the failure mode of walls in the RC-infill model was dominated by compression and bending; however, the failure mode of walls in the RCB-infill model was dominated by tension and compression in a diagonal direction. No obvious damage was observed at the beam-column joints in either model. The failure of the frame columns in the RC infill model was more severe than that in the RCB infill model, but the RC infill walls in the RCB-infill model suffered larger levels of damage than those in the RC-infill model, demonstrating the fully developed seismic capacity of the RC infill wall based on the protection of the RC infill wall mega braces (RCIWMBs).

Crack maps of the ultimate failure modes of the RCB-infill model and the RC-infill model are provided in Fig. 12. As seen from the crack patterns, the seismic damage degree of the frame structure was lighter in the RCB-infill model than in the RC-infill model. The frame structure was effectively protected after retrofitting with an RCIWMB.

4.3. Dynamic characteristics

The natural frequency and mode shape of the structure after each earthquake run were identified from the white-noise test data; moreover, the equivalent viscous damping ratio (EVDR) for the structure was calculated via the half-power bandwidth method. No torsional effect was found on the RCB-infill model, indicating that the entire rigidity and mass of the structure had a balanced distribution.

The first-order and second-order mode shapes of the two models in the X-direction are shown in Fig. 13. The first-order mode shape of the RC-infill model belongs to the shear-bending mode (Fig. 13a). The first-order mode shape of the RCB-infill model belongs to the shear mode, which is the same mode that supports a bare frame structure. The second-order mode shape (Fig. 13b) for the RC-infill model is similar to that of the RCB-infill model. Thus, the RC-infill model clearly transforms the shear deformation characteristics of the bare frame structure into a bending-shear type system, indicating that the structural system was changed. However, the addition of an RCIWMB did not change the shear deformation characteristics of the bare frame structure. This behavior is consistent with the deformation characteristics of a braced frame structure, revealing that the addition of an RCIWMB did not change the structural system of the frame structure; thus, the effect of the X-shaped mega braces is obvious. Therefore, the frame structure evaluation index can still be used in the RCB-infill model.

The global damage index of the structure is defined as $DI = 1 - (f_1/f_0)^2$. f_1 is the natural frequency after each earthquake motion, and f_0 is the initial natural frequency of the structure [31,32], which can be used to quantitatively compare the global structural damage experienced by the models during different tests. Fig. 14 shows the variation in the first-order natural frequencies, global damage indexes (DIs), and equivalent viscous damping ratios of the RC-infill model, as well as the RCB-infill model, in the X-direction.

The first-order natural frequency of the RCB-infill model was always higher than that of the RC-infill model in the entire phase of the test (Fig. 14a), indicating that the global stiffness of the RCB-infill model was larger than that of the RC-infill model because of the equal mass. Moreover, the initial natural frequency was 4.8 Hz for the RC-infill model and 5.6 Hz for the RCB-infill model, revealing that the global stiffness of the RCB-infill model increased by 36% compared with the RC-infill model. The DI value of the two models decreased progressively at almost the same rate (Fig. 14a), indicating that the local damage difference was not easy to capture using DIs. DIs can only macroscopically reveal the propagation of damage and the degradation of structural stiffness. Because the DI value is only related to frequency, the frequency was acquired under the low amplitude white noise tests. In the low-amplitude vibration, some damage to the structure was under the static friction state condition, and the frequency could not fully reflect the local damage.

Fig. 14b demonstrates the damping ratio variations of the two models in the X-direction. The damping ratio is an inherent structural property and depends on many influencing factors [32]. As shown in Fig. 14b, before the test at 800 gal, the initial damping ratio for the RCB-infill model was always less than that for the RC-infill model, which indicates that the RC-infill model is relatively flexible and that the RCB-infill model was not effectively mobilized enough to produce a damping force. After the PGA 800 gal test, the RCB-infill model's damping ratio exceeded that of the RC-infill model, which reveals that the RCB-infill model can have higher energy dissipation and alternative load-transfer paths, i.e., structural redundancy in the stage of a large earthquake.

4.4. Dynamic response

The main seismic behaviors of the RCB-infill model are presented in Figs. 15 to 18. The amplification factors of acceleration are defined as the ratio between the peak story accelerations of a given story and the base. The relative story displacement of the RC-infill model was calculated as the difference between the measured absolute story displacement and the base displacement. The interstory drift angle was calculated as the displacement difference divided by the height between two consecutive stories. The story shear force of the RCB-infill model was calculated by summing the inertia force of the stories above as follows:
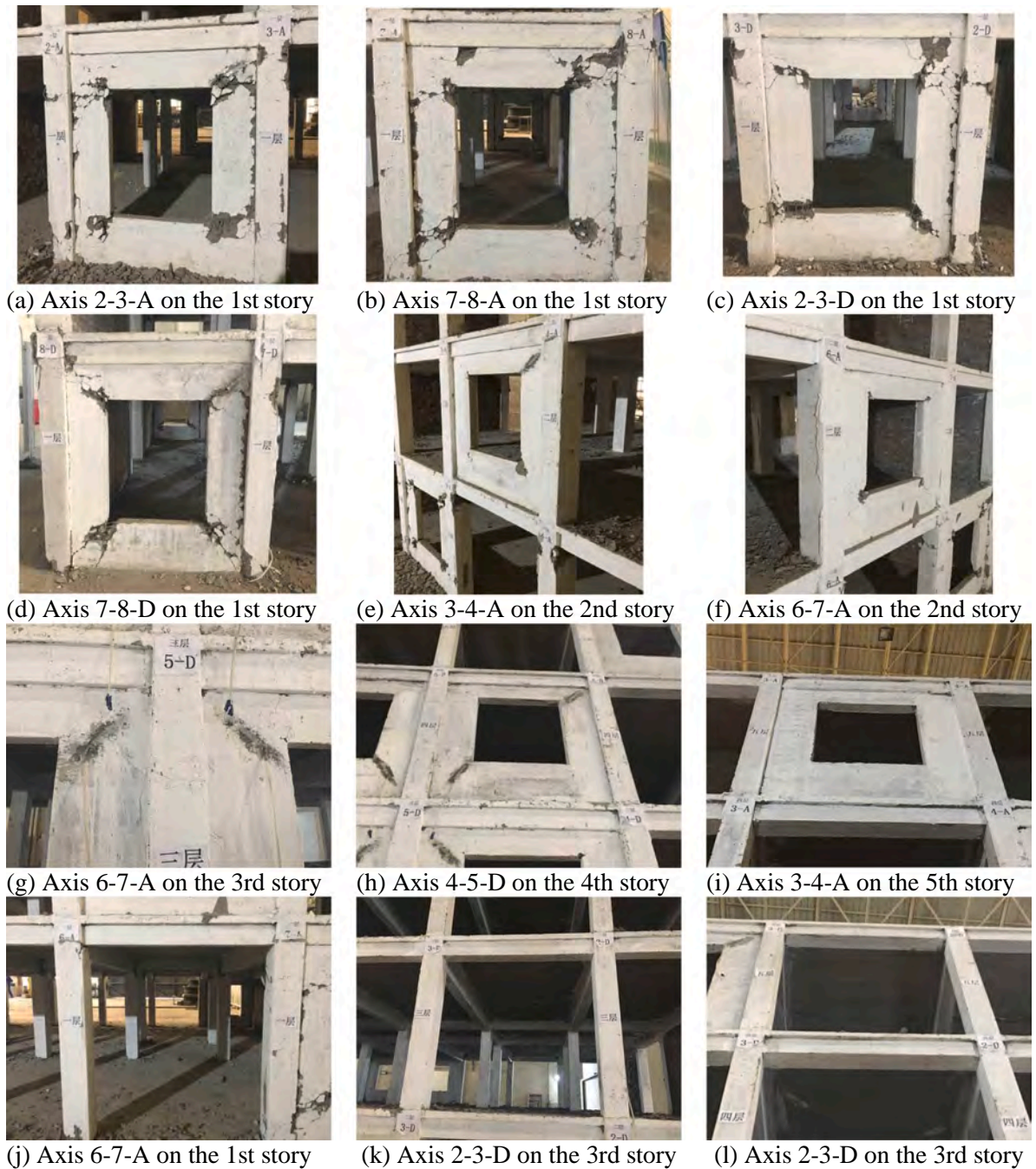
(a) Axis 2-3-A on the 1st story   (b) Axis 7-8-A on the 1st story   (c) Axis 2-3-D on the 1st story

(d) Axis 7-8-D on the 1st story   (e) Axis 3-4-A on the 2nd story   (f) Axis 6-7-A on the 2nd story

(g) Axis 6-7-A on the 3rd story   (h) Axis 4-5-D on the 4th story   (i) Axis 3-4-A on the 5th story

(j) Axis 6-7-A on the 1st story   (k) Axis 2-3-D on the 3rd story   (l) Axis 2-3-D on the 3rd story

Fig. 10. Typical cracks after the test at PGA = 1426 gal in the RCB-infill model.

$$V_j(t) = \max \left| \sum_{i=j}^{n} m_i a_i(t) \right| \tag{1}$$

where j is the story number; n is the number of the top story; $a_i(t)$ is the acceleration of story i at time t; m_i is the mass of story i; and $V_j(t)$ is the max story shear force of story j.

4.4.1. Acceleration responses

Fig. 15 shows the amplification coefficient of accelerations under different earthquake excitations at each floor of the RCB-infill model. As described in Fig. 15a and Fig. 15b, the acceleration responses of the RCB-infill model under different earthquake excitations are quite different at identical amplitudes. The acceleration response under the Taft wave was more violent than those under the other two waves during low-amplitude tests (with PGAs of 80.5 gal and 115 gal).

As the PGA of the Taft wave increased (Fig. 15c and Fig. 15d), the amplification factor decreased slightly as a result of the increase in damage and the damping force of the model, as well as the degradation of the model stiffness. During the test case with the PGA ranging from 80.5 to 230 gal, the shape of the acceleration amplification coefficient curve changed greatly. Elastic damage occurred, leading to a change in the structure's loading mechanism and a redistribution of the internal forces, especially in the first and fourth stories. During the test case, with the PGA ranging from 287.5 to 322 gal, the acceleration amplification coefficient of the upper four stories decreased continuously, revealing a gradual increase in damage to the upper four floors. After PGA = 460 gal, the acceleration amplification coefficient of the first story clearly decreased, showing that the damage was concentrated on the first story.
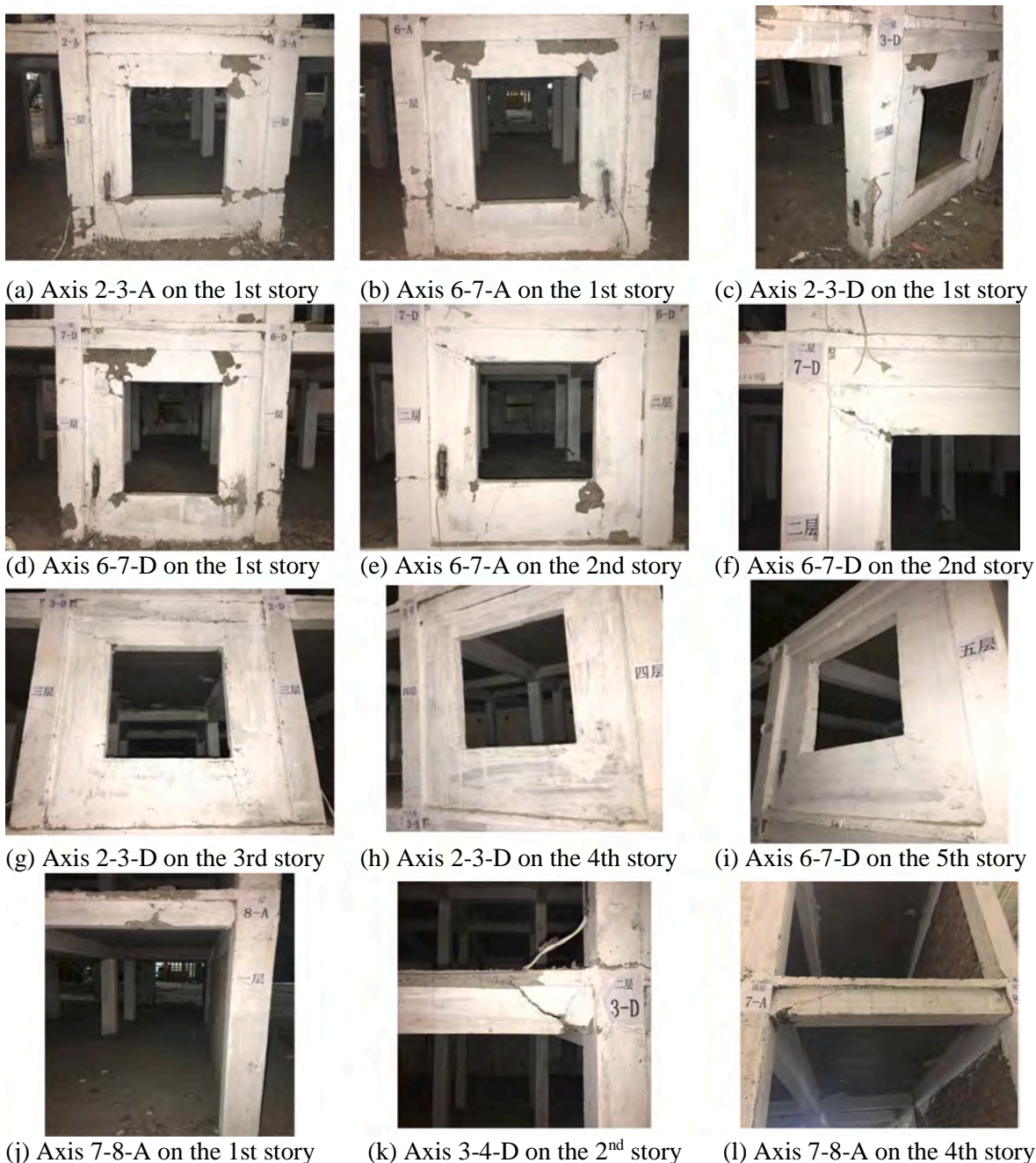
(a) Axis 2-3-A on the 1st story   (b) Axis 6-7-A on the 1st story   (c) Axis 2-3-D on the 1st story

(d) Axis 6-7-D on the 1st story   (e) Axis 6-7-A on the 2nd story   (f) Axis 6-7-D on the 2nd story

(g) Axis 2-3-D on the 3rd story   (h) Axis 2-3-D on the 4th story   (i) Axis 6-7-D on the 5th story

(j) Axis 7-8-A on the 1st story   (k) Axis 3-4-D on the 2nd story   (l) Axis 7-8-A on the 4th story

Fig. 11. Typical cracks after the test at PGA = 1426 gal in the RC-infill model.

Once again, the decrease in the acceleration amplification coefficient led to a change in the structure's loading mechanism. At PGA = 690 gal, the first-story acceleration amplification coefficient approached that of the previous test case. The acceleration amplification coefficient of the second and fourth stories decreased substantially. With the PGA ranging from 920 to 1426 gal, the shape of the acceleration amplification factor was basically similar, indicating that the damage level of the RCB-infill model increased gradually and the loading mechanism of the structure remained unchanged.

4.4.2. Displacement responses

For each story, the maximum displacement envelope curves of the RCB-infill model relative to that at the base are illustrated in Fig. 16. The maximum displacement response under the El Centro wave was the most violent when PGA = 80.5 gal (Fig. 16a). Clearly, the maximum

displacement occurred on the fourth story. The overall trend of the structural displacement was that of a shear mode, which is basically consistent with the first-order mode shape of the RCB-infill model. When the PGA reached 115 gal (Fig. 16b), the maximum displacement response occurred under the Taft wave, and the envelope curves of the maximum displacements retained their shear type classification. As the PGA increased, the maximum relevant displacements of each story also increased gradually (Fig. 16c and Fig. 16d). Thus, the maximum displacements occurred on the top story, and the curve shape of the displacements always retained its shear-type status throughout the Taft wave excitations.

Fig. 17 provides the maximum interstory drift angles of the RCB-infill model. Clearly, the maximum interstory drift angles of the RCB-infill model at PGA = 80.5 gal had the least impact, while the maximum interstory drift angle on the third story under the El Centro wave was 1/
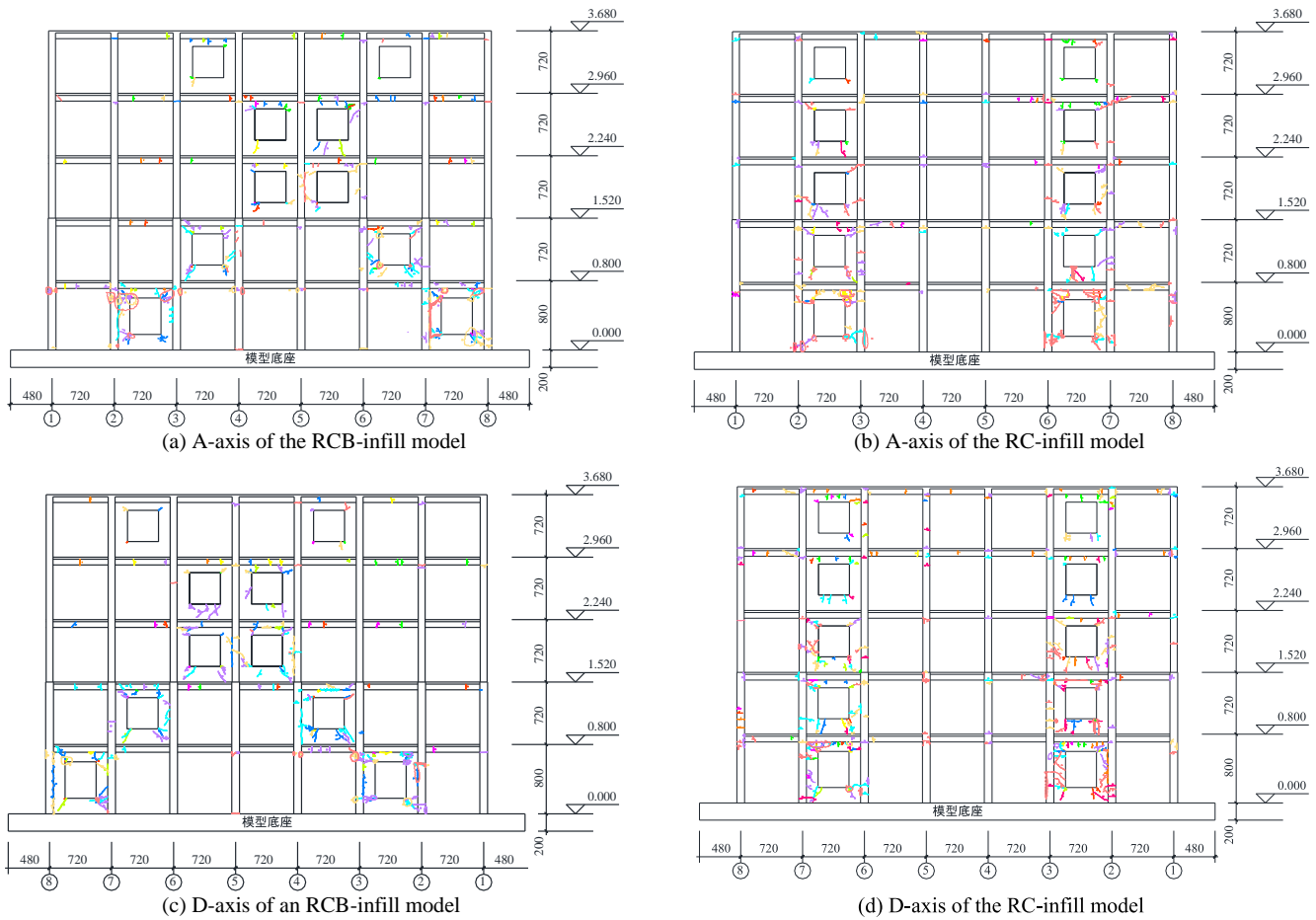
(a) A-axis of the RCB-infill model

(b) A-axis of the RC-infill model

(c) D-axis of an RCB-infill model

(d) D-axis of the RC-infill model

Fig. 12. Crack maps of ultimate failure modes.

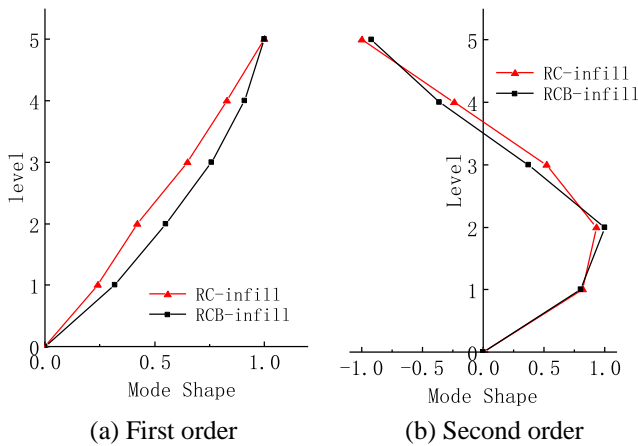(a) First order

(b) Second order

Fig. 13. The first two mode shapes.

803 (Fig. 17a), i.e., less than 1/550, defined as the elastic limit state for RC frame structures [20]. Hence, only slight damage occurred on the RC infills and the frame beams during this stage. After PGA = 115 gal, the maximum interstory drift angle occurred on the first story under the Taft wave at 1/639, which was less than the elastic limit state, and the distribution of the interstory drift was relatively uniform (Fig. 17b).

As the PGA of the Taft wave increased (Fig. 17c and d), the maximum interstory drift angles in the RCB-infill model increased. At the same time, the maximum interstory drift angle of the RCB-infill model exceeded the elastic limit state at PGA = 161 gal, which occurred on the

second story as 1/428. When the PGA reached 230 gal, the interstory drift angles of the first, fourth and fifth stories increased, and a weak story began to appear on the first story. After a PGA of 287.5 gal, the interstory drift angles of the RCB-infill model's lower three stories increased and those of the RCB-infill model's second and third stories were similar, indicating that the damage was concentrated in the lower three stories of the RCB-infill model in this stage. The interstory drift angles of the upper four stories were similar to that of the first story and were more disturbed at PGA = 322 gal. As the PGA increased to 460 gal, the interstory drift angles of the first story substantially increased. When the PGA reached 920 gal, the maximum interstory drift angles of the RCB-infill model exceeded the plastic drift limit of 1/50 recommended for RC frames [20].

4.4.3. Story shear force

Fig. 18 shows that story shear forces of the RCB-infill model increased from top to bottom, which is identical to a stepped distribution in ordinary buildings during low amplitude excitations. The story shear force increased with the PGA ranging from 80.5 to 920 gal, and the increase in shear force in each story was relatively uniform. When the PGA reached 1173 gal, the first and second story shear forces decreased suddenly and to a smaller extent than that of the previous test case, indicating that severe damage was concentrated on the first story, and the story stiffness had decreased. The story shear force of the lower three stories at PGA = 1426 was less than that of the lower three stories at PGA = 1173, revealing that the damage degree of the structure was further aggravated.
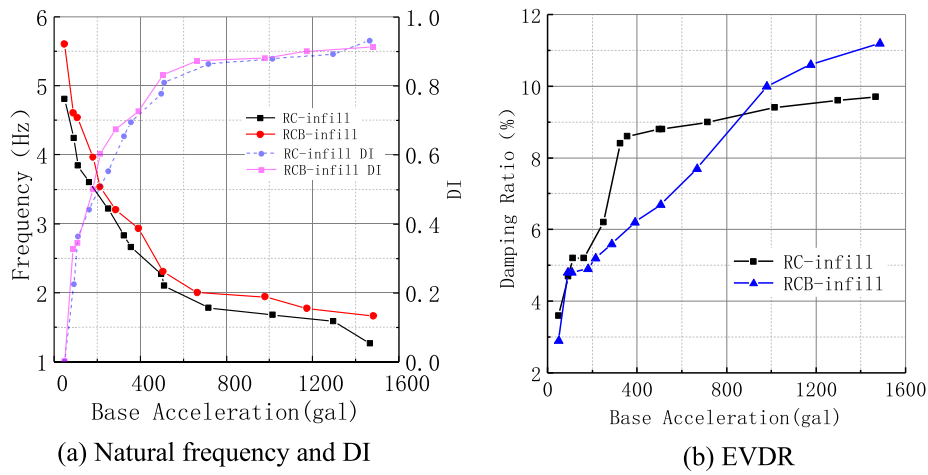
(a) Natural frequency and DI (b) EVDR

Fig. 14. Variation of dynamic characteristics.

(a) PGA=80.5 gal (b) PGA=115 gal (c) PGA=80.5–322 gal (d) PGA=322–1426 gal

Fig. 15. The amplification factors of acceleration.

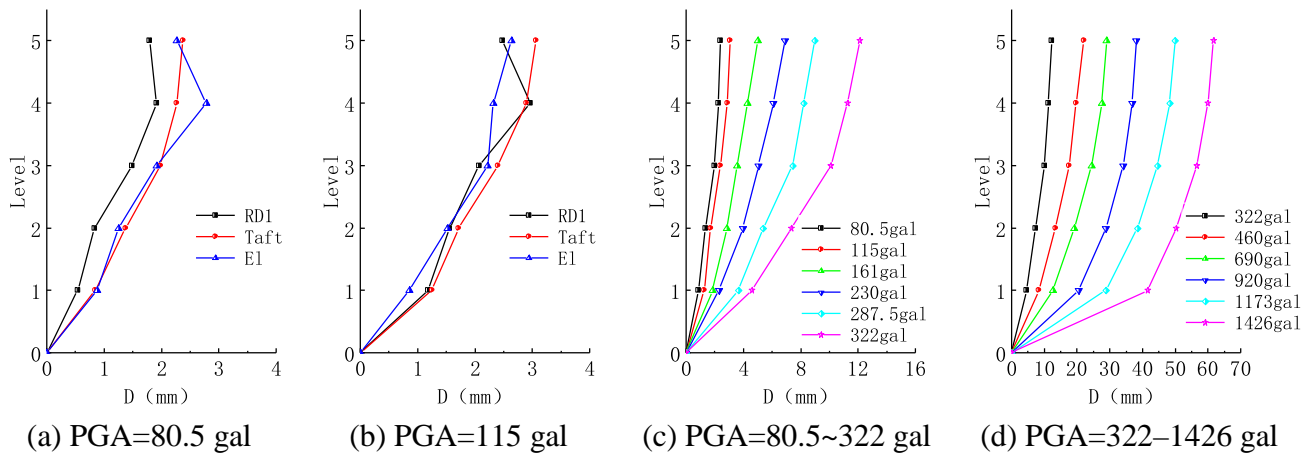(a) PGA=80.5 gal (b) PGA=115 gal (c) PGA=80.5~322 gal (d) PGA=322–1426 gal
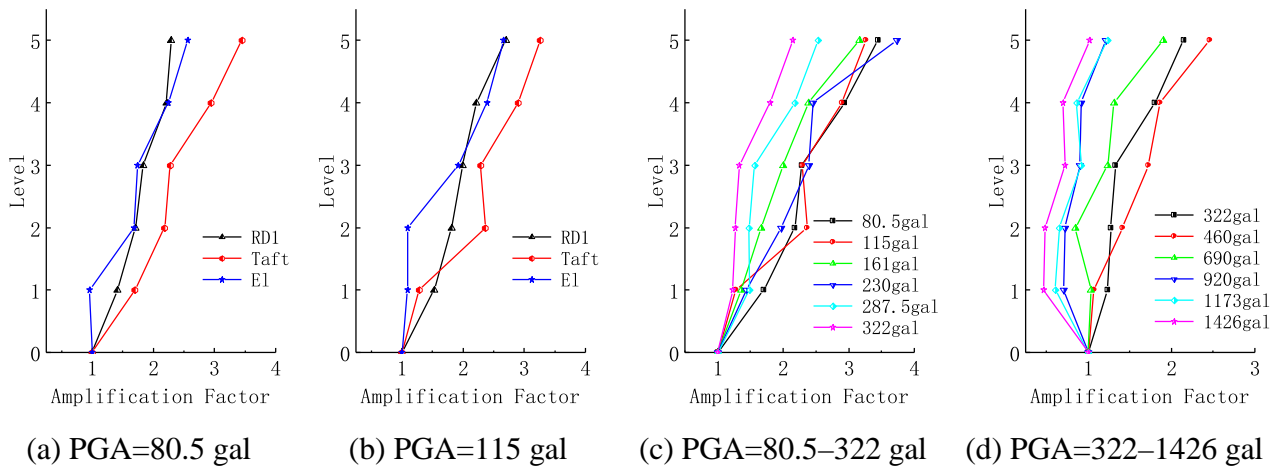
Fig. 16. Maximum relevant displacements.

4.4.4. Comparison of the two models

Fig. 19 depicts the maximum interstory drift angle of the RCB-infill model and RC-infill model. Based on the Taft wave input at different PGA levels, the maximum interstory drift angle in the upper four stories of the RCB-infill model was noticeably less than that of the RC-infill model during the all-inclusive tests, but the maximum interstory drift angle in the first story of the RCB-infill model was higher than that of the RCB-infill model after a PGA of 400 gal. This shows that introducing the RCIWMB can adequately limit the overall lateral deformation of the frame structure; however, the disadvantage of this scheme is the tendency to form a soft story mechanism in the bottom first story, and the structural story ductility of the first story is poor, which indicates that
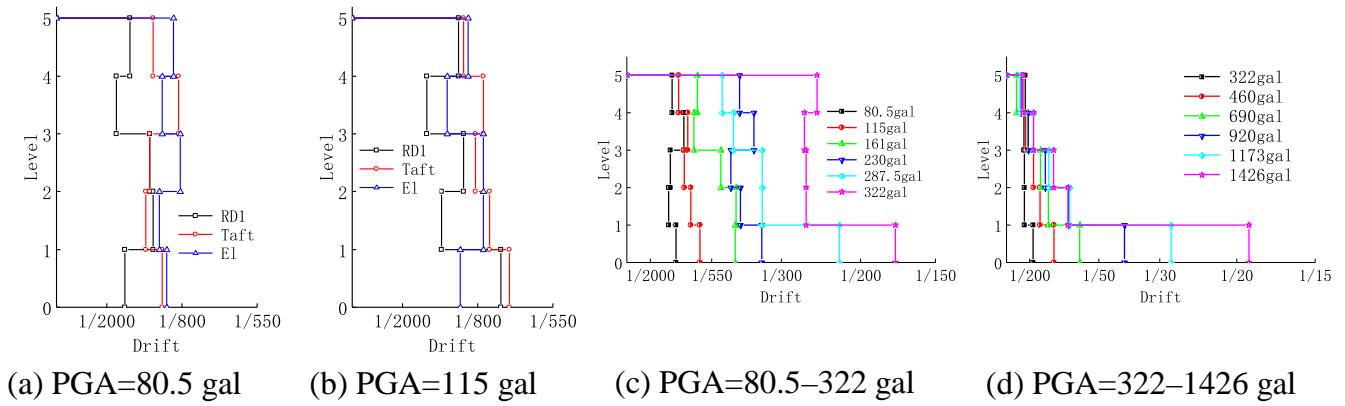
(a) PGA=80.5 gal   (b) PGA=115 gal   (c) PGA=80.5–322 gal   (d) PGA=322–1426 gal

Fig. 17. Maximum interstory drift angle.

(a) PGA=80.5 gal   (b) PGA=115 gal   (c) PGA=80.5–322 gal   (d) PGA=322–1426 gal
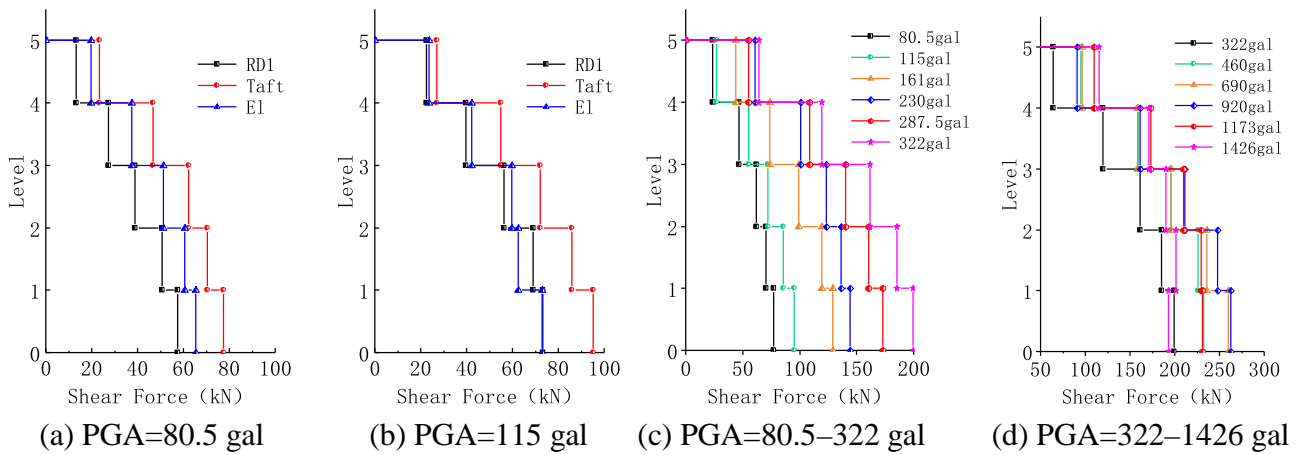
Fig. 18. Maximum story shear force.

the proposed diagonal arrangement of the infill walls is expected to produce more severe damage to the structure than the traditional arrangement. The degree of structural damage on the RCB-infill model gradually decreased from the bottom story to the top story. The RC infill wall was not fully developed in seismic capacity on the upper stories but was severely damaged on the bottom story. Hence, it is suggested that in engineering practice, the RC infill wall thickness can be reduced on the top stories and increased appropriately on the bottom to prevent the weak layer from appearing.

Fig. 20 presents the measured base shear force as it relates to the top story displacement curves (equivalent to a push-over curve) for the entire process of the two models, which can reflect the bearing capacity. The base shear force was the absolute peak shear force in the first story of the two models (that of the RCB-infill model is shown in Fig. 18). The results show that the bearing capacity of the RCB-infill model was substantially higher than that of the RC-infill model as long as the top story displacement was less than 40 mm. After the top story displacement exceeded 40 mm, the bearing capacity of the RCB-infill model decreased rapidly. To determine the yield point, we used the method proposed by Park [33]; thus, the displacement corresponding to the 85% peak load at the falling section of the skeleton curve was taken as the ultimate displacement. The ductility coefficient was taken as the ratio between the ultimate displacement (Δu) and the yield displacement (Δy). The yield displacement and the ultimate displacement of the RC-infill model were 32.98 mm and 79.03 mm, respectively. The displacement ductility of the RC-infill model was 2.39. The yield displacement and the ultimate displacement of the RCB-infill model were 15.8 mm and 52.37 mm, respectively. The displacement ductility of the RCB-infill model was 3.31. These results show that the RCB-infill

model has a good bearing capacity and good integral ductile behavior.

4.5. Seismic performance objectives analysis

Because the structural systems of the RCB-infill model and the RC model differ in terms of interstory drift, the RC-infill model should adopt the control index of the frame-shear wall structure. However, the RCB-infill model should adopt the control index of the frame structure because of the lack of changes in the structural system. Therefore, the seismic performance of the RCB-infill model is only discussed in this section.

To comprehensively understand the seismic performance of the RCB-infill model, the capacity spectrum method is used. Fig. 21a and b depict the comparison curves between the capacity spectrum and the corresponding demand spectrum of the model fortified to meet the demand of 7-degree and 8-degree earthquakes [20], respectively. The spectral accelerations and displacements were obtained from the displacement-force curve shown in Fig. 19 according to the method suggested in [34]. The damping coefficients of 7-degree and 8-degree earthquakes were 18% and 20%, respectively. The calculation formula is expressed as:

$$\xi_{eq} = \frac{0.637(a_y d_{pi} - d_y a_{pi})}{a_{pi} d_{pi}} + 0.05 \tag{2}$$

where a_y represents the spectral acceleration of the initial yield point; d_y represents the spectral displacement of the initial yield point; a_{pi} represents the spectral acceleration of the corresponding loading point; and d_{pi} represents the spectral displacement of the corresponding loading
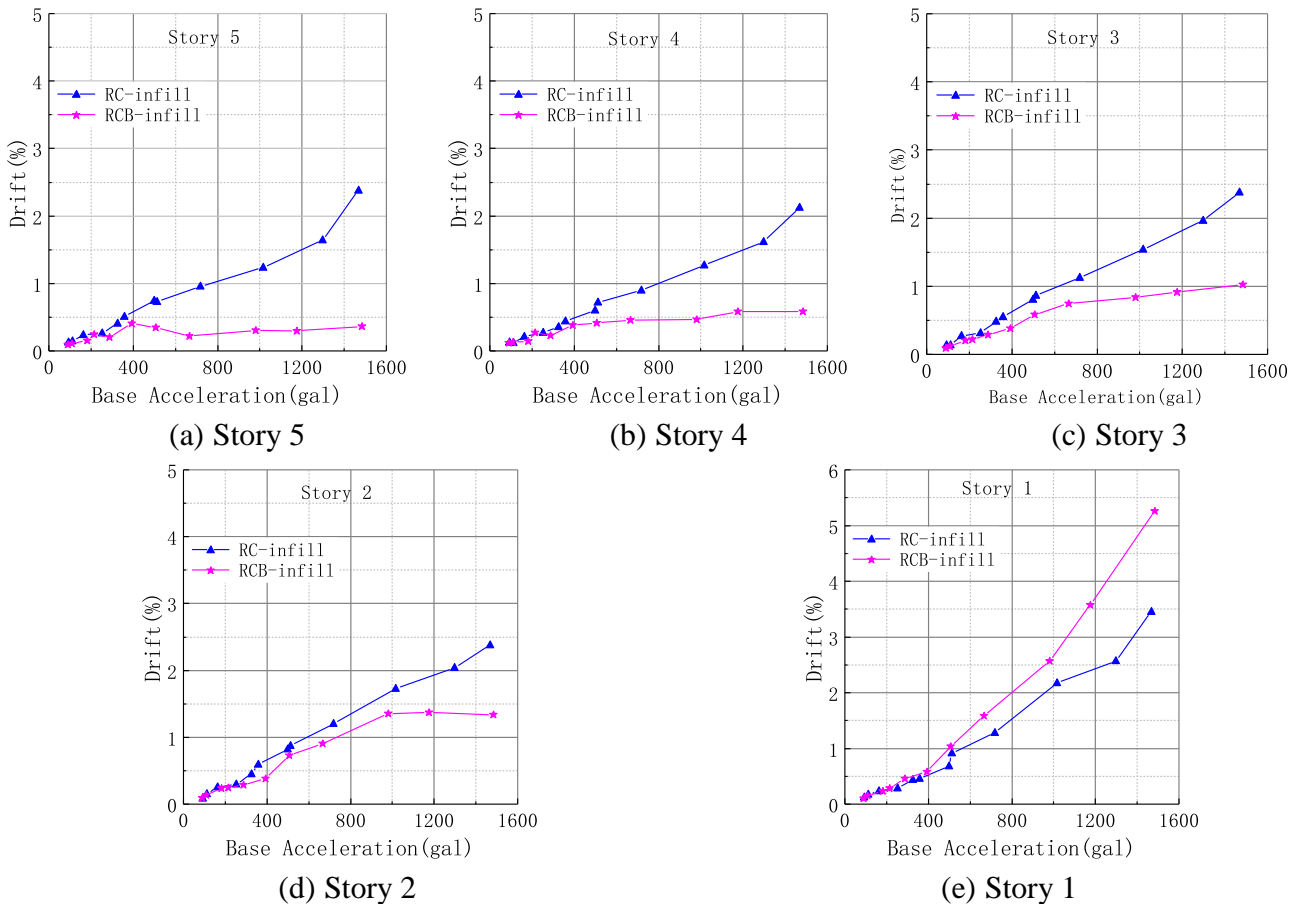
(a) Story 5   (b) Story 4   (c) Story 3

(d) Story 2   (e) Story 1

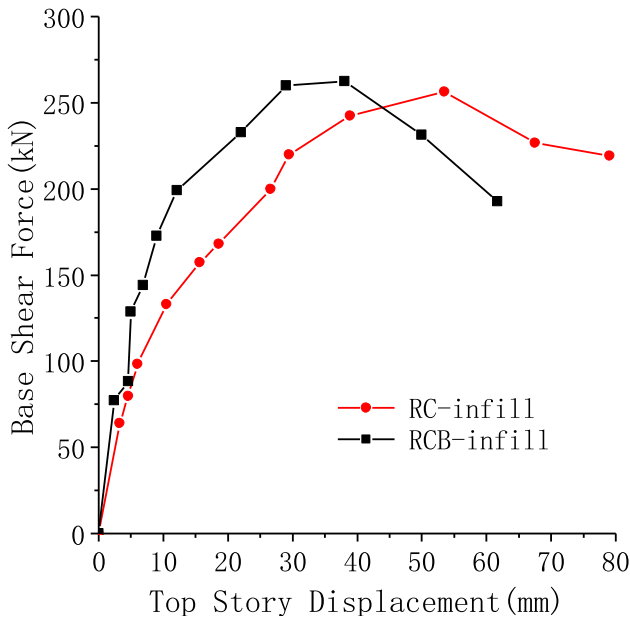**Fig. 19.** Maximum interstory drift under the Taft wave.

Fig. 20. Top story displacement comparison with base shear force curves.

point.

The capacity-demand spectrum curves of the 7-degree seismic fortification are depicted in Fig. 21a as corresponding to the characteristic response points of frequent earthquakes, which are far less than

the spectral displacement and acceleration corresponding to 80.5-gal excitations. Thus, the maximum interstory drift of the RCB-infill model on the fourth floor was 1/823 at a PGA of 80.5 gal. The value of the maximum interstory drift corresponding to the characteristic response points of frequent earthquakes was much less than the elastic limit drift of 1/550, which corresponded to the characteristic response points of rare earthquakes. The RCB-infill model's maximum interstory drift value was slightly closer to the spectral acceleration and displacement corresponding to the 287.5-gal excitations. The RCB-infill model's first-story maximum interstory drift was 1/220 at PGA = 287.5 gal; therefore, the value of the maximum interstory drift corresponding to the characteristic response points of rare earthquakes was much less than the plastic limit drift of 1/50. Based on these results, the seismic retrofitting RC frames with the RCIWMB can meet the demand of 7-degree fortification.

The capacity-demand spectrum curves of 8-degree seismic fortification are depicted in Fig. 21b, corresponding to the characteristic response points of frequent earthquakes. These response points are slightly less than the spectral displacement. When responding to an acceleration corresponding to 115-gal excitations, the maximum interstory drift of the first-story RCB-infill model was 1/639 at PGA = 115 gal; therefore, the value of the maximum interstory drift corresponding to the characteristic response points of frequent earthquakes is much less than the elastic limit drift of 1/550, which corresponds to the characteristic response points of rare earthquakes. The maximum interstory drift is slightly closer to the spectral acceleration and displacement corresponding to 460-gal excitations. The maximum interstory drift of the RCB-infill model was 1/97 in the first story at a PGA of 460 gal. Therefore, the value of the maximum interstory drift corresponding to the characteristic response points of rare earthquakes is much less than
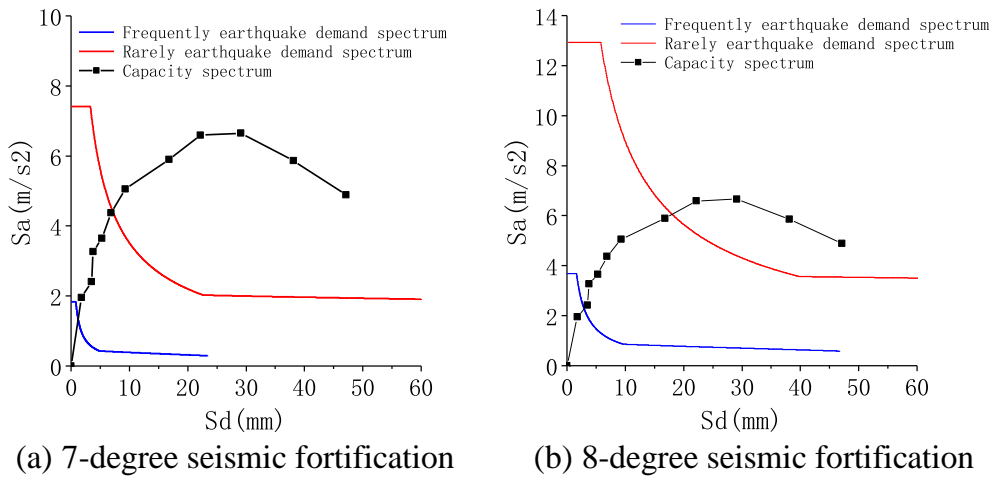
(a) 7-degree seismic fortification

(b) 8-degree seismic fortification

Fig. 21. Capacity-demand spectrum curves.

the plastic limit drift of 1/50. Based on these results, the seismic retro-fitting of RC frames with the RCIWMB can meet the 8-degree fortifica-tion demand.

4.6. Structural dynamic strain analysis

After the counterweight was loaded, the measured strain value from strainmeters was recorded and then reset to zero before the test. Fig. 22 provides an overview of the time history responses of strains in the frame columns by plotting the recorded strains at the bottom end of the

columns. SL5 and SL12 represent the strains of ordinary columns not adjacent to RC infill walls on the first and third stories, respectively. SL8 and SL10 represent the strain at the connected columns adjacent to RC infill walls on the first and third stories, respectively. The strain values increased as the PGAs ranged from 80.5 gal to 230 gal. Furthermore, the connected column strain values were larger than those of the ordinary frame columns on the same story. After the PGA reached 287.5 gal, the residual strain began to occur at connected columns on the first story and tended to be stable, indicating that the connected column was damaged or destroyed. When the PGA reached 322 gal, the strain at the
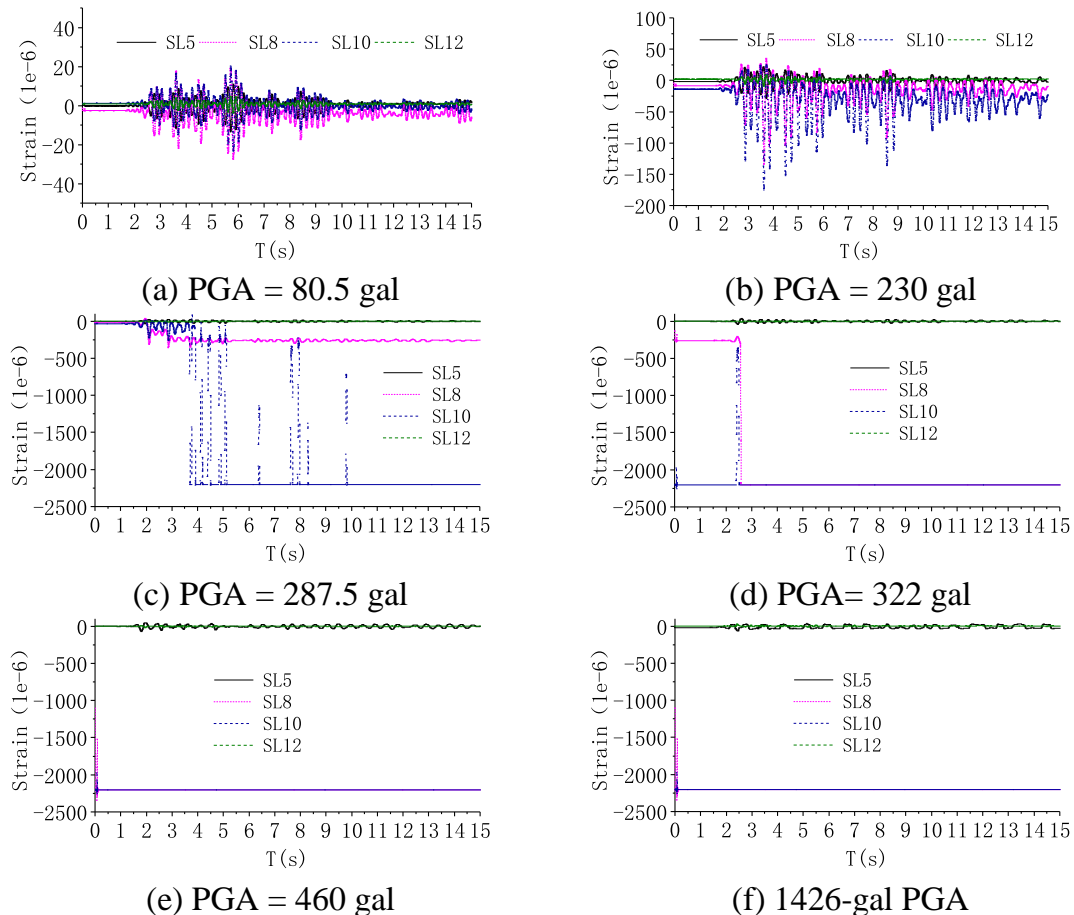

(a) PGA = 80.5 gal

(b) PGA = 230 gal

(c) PGA = 287.5 gal

(d) PGA= 322 gal

(e) PGA = 460 gal

(f) 1426-gal PGA

Fig. 22. Recorded time history responses of strains at the bottom end of columns.

connected column of the first story had a sudden increase, indicating that brittle failure had occurred. The strain of the ordinary columns still fluctuated with the input ground motion. This chain of events starting with the brittle failure of connected columns on the first story up to the fluctuation of ordinary columns responding to the input ground motion led to the RC infill walls adjacent frame columns also failing. During the test case with PGAs ranging from 460 to 1426 gal, the strains at the connected columns did not change because of shear failure; moreover, the strain of the ordinary columns continued to fluctuate, indicating no shear failure at the ordinary columns. Their failure was dominated by flexural failure, which is consistent with the experimental phenomenon.

Some recorded strains at the bottom of the RC infill walls in the RCB-infill model are demonstrated in Fig. 23. The strain of RC infill walls increased with increasing PGA levels. In the low amplitude excitation (PGA = 80.5–230 gal), the fourth-story strains (SL30) were higher than those of the other stories. With PGAs ranging from 287.5 to 322 gal, the fourth-story strains (SL28 and SL30) were higher than those of the other stories. Before PGA = 322 gal, because the layout of RC walls in the third and fourth stories was relatively concentrated, complex structure stress resulted in large diagonal deformation on the fourth floor. The internal

force redistributed with the growing damage. During the test case with the PGA ranging from 460 to 690 gal, the third-story strain (SL24 and SL27) increased sharply, and large residual deformation occurred; thus, strain SL27 rapidly reached its maximum damage level and remained unchanged at PGA = 690 gal, showing that the RC wall corners cracked at this stage. When the PGA reached 920 gal, the strains (SL21, SL26 and SL30) increased rapidly and remained unchanged, indicating that several RC infill walls had been damaged or destroyed. With PGAs ranging from 1173 to 1426 gal, the structure was ultimately destroyed as strainmeters in the damaged part of the structure failed, with only the fifth-story strains recorded as small. The strain levels of the third and fourth stories were higher. The second-story strain level was lower, and the fifth-floor strain level was the lowest. A comparative analysis of the structure's dynamic strain time history revealed that the structural stress was relatively concentrated for densely distributed RC infill walls, which resulted in large structural deformation.

4.7. Sa–Sd hysteresis of an equivalent single-degree-of-freedom system

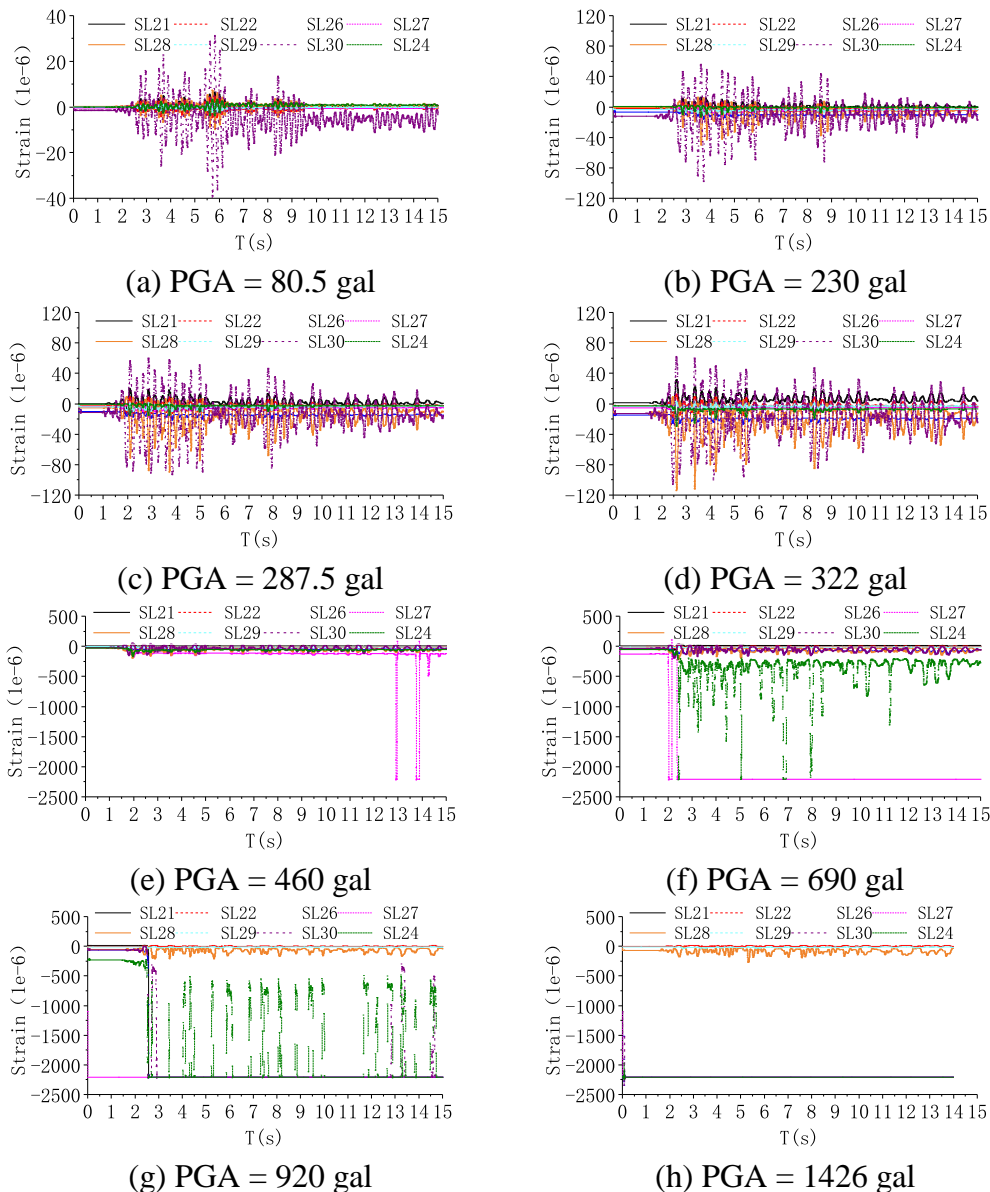For ease of applicability, the hysteretic response of the multistory

Fig. 23. Recorded time-history responses of strains at the bottom of RC infill walls.

specimen can be represented by equivalent single-degree of freedom (ESDOF) systems. A straightforward procedure was used to transform the multidegree-of-freedom system to an ESDOF system. ESDOF systems can sufficiently represent the overall dynamic response of the first-mode dominated actual structure [35]. The basics of the transformation procedure can be concisely expressed as:

$$S_d(t) = \frac{\Sigma_{i=1}^{N} m_i \varphi_i d_i(t) \gamma_1}{\Sigma_{i=1}^{N} m_i \varphi_i \gamma_1} \tag{3}$$

$$S_a(t) = \frac{\Sigma_{i=1}^{N} V_i(t) \varphi_i S_d(t) \gamma_1}{\Sigma_{i=1}^{N} m_i \varphi_i S_d(t) \gamma_1} \tag{4}$$

where $S_d(t)$ is the spectral displacement; $S_a(t)$ is the spectral acceleration; $d_i(t)$ is the structural displacement of a certain story; i is the number of stories; Φ_i denotes the mode shapes of the first mode; γ_1 is the first mode participation factor; and $V(t)$ is the story shear force.

Fig. 24 shows the variations in the first-order mode shapes of the RCB-infill model under different levels of PGA. The variation in the response characteristics of the RCB-infill model under different PGAs is illustrated in Fig. 25. At a PGA of 80.5 gal, the total area value of the hysteresis curve is considered an RD1 excitation accompanied by Taft and El Centro excitations of 4.92, 15.45 and 9.49 (mm·m/s²), respectively. At a PGA of 115 gal, the total area value of the hysteresis curve is considered an RD1 excitation accompanied by Taft and El Centro excitations of 13.87, 31.34 and 11.5 (mm·m/s2), respectively. These data revealed that the RCB-infill model consumed the most energy under Taft excitation. The Sa-Sd hysteresis curves were distributed in a thin, straight line, and the inclination of the curves remained similar at PGA rates of 80.5 gal and 115 gal, indicating an elastic stage.

Fig. 26 shows variations in the RCB-infill model response characteristics under different PGA levels of the Taft excitations. With PGAs ranging from 80.5 to 287.5 gal, the area of the hysteresis curve increased slowly. The inclination of the curve did not change substantially, showing slight degradation of structural stiffness. With PGAs ranging from 322 to 690 gal, the hysteresis curve area increased rapidly, and the inclination of the curve changed substantially as the stiffness degradation advanced relatively quickly during this stage. At this point, the RCB-infill model entered the elastic–plastic stage and consumed more energy. During the test case with the PGA ranging from 920 to 1426 gal, the area of the hysteresis curve first increased and then decreased. The peak area occurred at a PGA of 1173 gal, which was 1.21e3 (mm·m/s2). Here, the inclination of the curve demonstrably decreased, and the stiffness degradation was severe. This demonstrated that the energy dissipation capacity of the RCB-infill model reached its maximum capacity at PGA = 1173 gal. After PGA = 1173 gal, the structural damage was aggravated, the energy dissipation capacity gradually decreased, and the structure was on the verge of collapse.

5. Conclusions

In this study, the seismic behavior of RC frames retrofitted by RC infill wall mega braces (RCIWMBs) was investigated using a 1/5-scale shaking table test. In addition, the test results were compared with those of a traditional RC infill wall retrofitted frame structure. The following conclusions were drawn based on the following experimental setups.

(1) The number of added RC infill walls was identical in both types of frame structures. The RC wall frame was filled with staggered diagonal RC-infill walls with mega braces (RCIWMBs) placed in a continuous arrangement connected to the frame members through dowel bars all around its perimeter from the bottom story to the top story, thereby providing higher lateral stiffness than that of the traditional arrangement of the RC wall. The bracing effect was obvious.

(2) The addition of an RC infill wall using the traditional arrangement changes the structural system. The mode shape curve and the structural deformation characteristics changed from shear type to bending-shear type; therefore, the deformation control index of the frame-shear wall structure is sufficiently exemplary for recommendation as part of the frame-RCIWMB retrofitted wall setup because it does not change the structural system. Furthermore, the mode shape curve and the structural deformation characteristics are still considered part of the shear type frame-to-wall structure. The deformation control index of the frame structure should be adopted after retrofitting.

(3) Compared with traditional RC infill wall retrofitted frame structures, the frame structure retrofitted by RC infill wall mega braces (RCIWMBs) played a large role in the increased integral lateral bearing capacity, integral lateral stiffness, and integral ductility. These findings suggest that the staggered diagonal continuous arrangement of RCB-infill walls can greatly improve the integral lateral stiffness, integral ductility, and integral bearing capacity of a structure and limit the lateral deformation of the structure. However, a poor structural story ductility of the first story can be noticed, as the story drift ratios of the first story of the RCB-infill model are substantially larger than those of the traditional model, which indicates that the proposed diagonal arrangement of the infill walls should produce more severe damage to the integral structure than the traditional arrangement.

(4) When the frame structure is retrofitted by RC infill wall mega braces, the damage is primarily concentrated in the RC infill walls, while the damage to the original frame structural members is light. Therefore, the RC infill wall mega braces can be used as the first seismic line of defense to reduce the damage of the original frame structure in earthquakes. Another benefit is that RC infill wall mega braces are easy to repair and replace after earthquakes.

(5) An analysis of the capability demand spectrum showed that the seismic behavior of the frame structure retrofitted by RC infill wall mega braces can meet the demand of 7-degree and 8-degree fortifications, according to the Chinese seismic code.

(6) The hysteretic response of the frame structure retrofitted by RC infill wall mega braces was analyzed via the equivalent single degree of freedom hysteretic Sa-Sd curve. Clearly, the inclination of the curve under minor earthquakes is large, the elastic stiffness is higher, and the energy consumption is less. Under moderate earthquakes and major earthquakes, the area of the hysteretic curve increased gradually, and more energy was consumed, demonstrating the structure's good energy dissipation capacity.
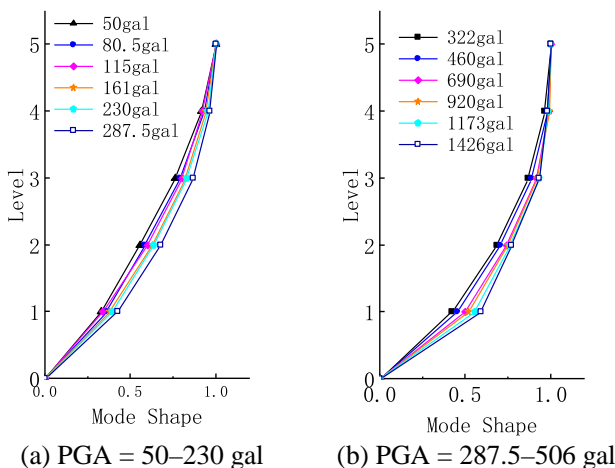

(a) PGA = 50–230 gal   (b) PGA = 287.5–506 gal

Fig. 24. Variation of the first-order mode shapes.

(a) PGA = 80.5 gal   (b) PGA = 115 gal
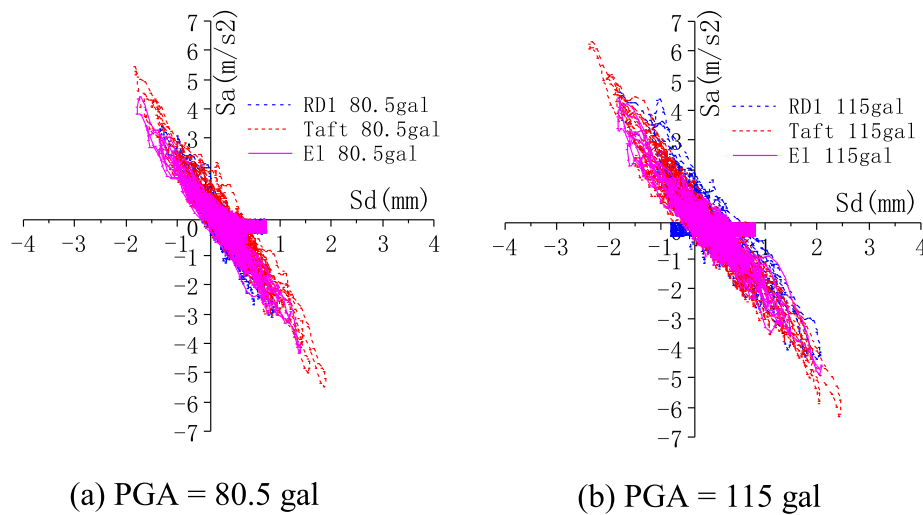
Fig. 25. Sa-Sd hysteresis curves under different earthquakes.

(a) PGA = 161~287.5 gal   (b) PGA = 322~690 gal   (c) PGA = 920~1426 gal
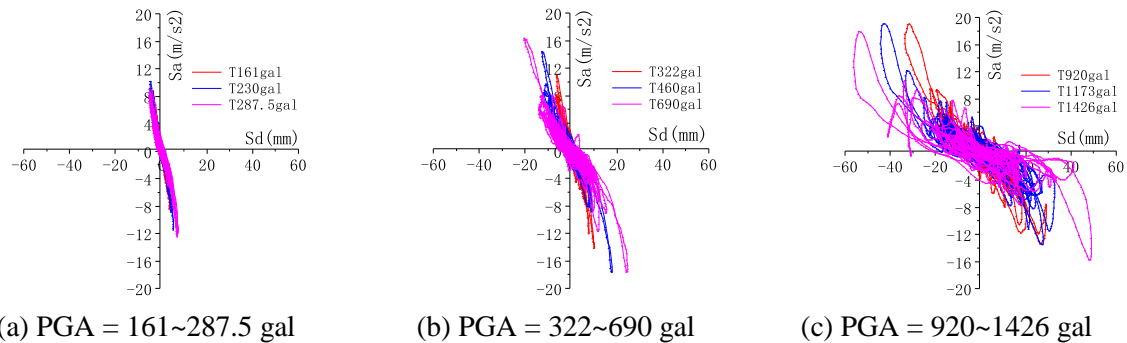
Fig. 26. Sa-Sd hysteresis curves under different levels of PGA.

(7) Attention was focused on the damage concentrations on the third and fourth stories with densely distributed RC walls and the first story's frame structure reinforcement supported by the RC infill wall mega braces. To avoid nonductile failures of the connected frame columns and the formation of soft story mechanics, two recommendations were given: (1) The ductility of the column can be improved by increasing the cross-section of the connected frame columns or strengthening with FRP material, and (2) setting the stiffness of each layer allows a reasonable change to the magnitude of the seismic force and prevents the weak layer from appearing. This also occurs when adjusting the thickness of the added RC infill walls from the top layer to the bottom layer. Plans for a deeper study are being made to optimize this technique in ongoing research.

CRediT authorship contribution statement

Shao-Ge Cheng: Methodology, Conceptualization, Project administration, Funding acquisition. **Yi-Xiu Zhu:** Investigation, Data curation, Writing - original draft. **Wei-Ping Zhang:** Writing - review & editing. **Tie-Hua Shi:** Supervision, Validation.

Declaration of Competing Interest

The authors declare that they have no known competing financial interests or personal relationships that could have appeared to influence the work reported in this paper.

References

[1] Belleri A, Brunesi E, Nascimbene R, Pagani M, Riva P. Seismic performance of precast industrial facilities following major earthquakes in the Italian territory. J Perform Constr Facil 2015. https://doi.org/10.1061/(ASCE)CF.1943-5509.0000617,04014135.

[2] Civil and Structural Groups of Tsinghua University, XinanJiaotong University and BeijingJiaotong University. Analysis on seismic damage of buildings in the Wenchuan earthquake. J Build Struct. 2008;29(4):1–9.

[3] Stazi F, Serpilli M, Maracchini G, Pavone A. An experimental and numerical study on CLT panels used as infill shear walls for RC buildings retrofit. Constr Build Mater 2019;211:605–16.

[4] Hadigheh SA, Mahini SS, Maheri MR. Seismic behavior of FRP-retrofitted reinforced concrete Frames. J Earthquake Eng 2014;18:1171–97.

[5] Ruiz SE, Santos-Santiago MA, Bojórquez E, Orellana MA, Valenzuela-Beltrán F. BRB Retrofit of mid-rise soft-first-story RC moment-frame buildings with masonry

infill in upperstories. J Buildi Eng 2020. https://doi.org/10.1016/j.jobe.2020.101783.

[6] Eldin Mohamed Nour, Dereje Assefa Jonathan, Kim Jinkoo. Seismic retrofit of RC buildings using self-centering PC frames with frictiondampers. 109925 Eng Struct 2020;108. https://doi.org/10.1016/j.engstruct.2019.109925.

[7] Javadi Pasha, Yamakawa Tetsuo. Strength and ductility type retrofit of soft-first-story RC frames through the steel-jacketed non-reinforced thick hybrid wall. Eng Struct 2019;186:255–69.

[8] Frosch RJ, Wanzhi L, Jirsa JO, Kreger ME. Retrofit of non-ductile moment-resisting frames using precast infill wall panels. Earthquake Spectra 1996;12(4):741–60.

[9] Sonuvar M, Ozcebe G, Ersoy U. Rehabilitation of reinforced concrete frames with reinforced concrete infills. ACI Struct J 2004;101(4):494–500.

[10] Erdem I, Akyuz U, Ersoy U, Ozcebe G. An experimental study of two different strengthening techniques for RC frames. Eng Struct 2006;28(13):1843–51.

[11] Kaplan H, Yilmaz S, Cetinkaya N, Atimtay E. Seismic strengthening of RC structures with exterior shear walls. Sadhana 2011;36(1):17–34.

[12] Korkmaz HH. Seismic performance improvement of reinforced concrete frames not designed according to TDY 2007 with external shear walls. Project No. 11101012, Selcuk Univ., Scientific Research Projects Office (BAP), Konya, Turkey. 2013.

[13] Yunus D. Assessing a retrofitting method for existing RC buildings with low seismic capacity in turkey. J Perform Constr Facil 2017;31(2):04016098.

[14] Elias S, Xenophon P, Fardis Stathis NB. Experimental Investigation of Concrete Frames Infilled with rc for Seismic Rehabilitation. J Struct Eng 2014;140:04013033.

[15] Rao KNVP. Staggered shear panels in tall buildings. J Struct Eng 1983;109(5):1174–93.

[16] Tong YF. Study on the arrangement of shear wall in frame shear wall structure. J Build Struct 1983;02:70–2.

[17] Liu JX, Wang HN, Li P, Zhu MC. Experiment study and nonlinear analysis of a new skip-floor staggered shear wall structure for high-rise buildings. Appl Mech Materi 2013;351–352:131–7.

[18] Dong ZP. Research on mechanical properties of staggered shear wall structure, Master's thesis: Department of Civil Engineering, Northeast Forestry University, 2016.

[19] Tang XR, Shen P. Experimental study on the seismic behavior of reinforced concrete staggered shear wall structures. Sichuan Build Sci 2008;34(06):138–44.

[20] National Standard of the People's Republic of China. GB50011-2010 code for seismic design of buildings. Beijing: China Architecture and Building Press; 2010 [in Chinese].

[21] National Standard of the People's Republic of China. GB50010-2010 code for design of concrete structures. Beijing, China: China Architecture and Building Press; 2010 [in Chinese].

[22] National Standard of the People's Republic of China. TJ11-74 aseismic code of industrial and civil building. Beijing. 1974. [in Chinese].

[23] Shaoge Cheng, Xin Yang, Yixiu Zhu, Weiping Zhang. Study on simulation law of shaking table test based on equivalent yield strength coefficient. Earthquake Eng Struct Dyn 2020;40(5):1–10 [in Chinese].

[24] Qiao Yu-Meng, Lu Da-Gang, Yu Xiao-Hui. Shaking table tests of a reinforced concrete frame subjected to mainshock-aftershock sequences. J Earthquake Eng 2020. https://doi.org/10.1080/13632469.2020.1733710.

[25] Lu Zheng, Chen Xiaoyi, Lu Xilin, Yang Zi. Shaking table test and numerical simulation of an RC frame-core tube structure for earthquake-induced collapse. Earthq Eng Struct Dyn 2016;45:1537–56. https://doi.org/10.1002/eqe.2723.

[26] Shen Chaoyong, Zhou Fulin, Huang Xiangyun, Luo Xuehai, Ren Min, Chen Jianqiu, Wang Yu. Experimental research on mircroconcrete used in dynamic test model. J Guangzhou Univ (Natural Sci Ed) 2005;3(4):249–53.

[27] Nayak Diptiranjan, Pattnaik Rashmi R, Bhoi Kailash C, Panda Bikash C. Investigation into material strength and direction of applied forces to assess bonding behaviour of micro-concrete. J Instit Eng (India): Series A 2019;100(1):75–82.

[28] National Standard of the People's Republic of China. JGJ3-2010. Technical specification for concrete structures of tall building. Beijing: China Construction Press; 2010. [in Chinese].

[29] Žarnić Roko, Gostič Samo, Crewe Adam J, Taylor Colin A. Shaking table tests of 1:4 reduced-scale models of masonry infilled reinforced concrete frame buildings. Earthq Eng Struct Dyn 2001;30(6):819–34.

[30] Tan Kok Tong, Razak Hashim Abdul, Lu Dagang, Li Yanjun. Seismic response of a four-storey RC school building with masonry-infilled walls. Nat Hazards 2015;78:141–53.

[31] DiPasquale E, Ju J, Askar A, Çakmak AS. Relation between global damage indices and local stiffness degradation. J Struct Eng 1990;116(5):1440–56.

[32] Reyes Garcia, Iman Hajirasouliha, Maurizio Guadagnini, Yasser Helal, Yaser Jemaa, Kypros Pilakoutas, et al. Full-Scale shaking table tests on a substandard RC building repaired and strengthened with post-tensioned metal straps. J Earthq Eng. 2014;18(2):187–213.

[33] Park R. Evaluation of ductility of structures and structural assemblages from laboratory testing. Bull New Zealand National Soc Earthq Eng 1998;22(3):155–66.

[34] Applied Technology Council (ATC-40). Seismic evaluation and retrofit of concrete buildings, Redwood City, California. 1996.

[35] Cem Y, Ryo Y, Takuya N, Kenichi T, Yusuke T, Koichi K, et al. Shake table test of a full-scale four-story reinforced concrete structure and numerical representation of overall response with modified IMK model. Bull Earthq Eng 2018;16(5):2087–211.